Phosphonate Lipid Tubules. 1

B. N. Thomas,* R. C. Corcoran, C. L. Cotant, C. M. Lindemann, J. E. Kirsch, and P. J. Persichini

Contribution from the Department of Chemistry, The University of Wyoming, Laramie, Wyoming 82071-3838

Received November 17, 1997. Revised Manuscript Received September 22, 1998

Abstract: We describe a new chiral tubule-forming lipid in which the C−O−P headgroup/glycerol backbone linkage of the archetypal tubule-forming phospholipid, 1,2-bis(10,12-tricosadiynoyl)-*sn*-glycero-3-phosphocholine, DC(8,9)PC, is replaced by a C−C−P linkage. Tubule formation from this phosphonate analogue occurs under the same mild conditions as with DC(8,9)PC and produces identical yields, but the phosphonate tubules have cylindrical diameters twice that of DC(8,9)PC tubules. Small-angle X-ray scattering, atomic-force, and optical microscopy reveal the new tubules to consist of fewer coaxially nested cylindrical lamellae than DC(8,9)PC tubules; accordingly, the phosphonate tubules are more fragile. In addition, a small portion of the phosphonate precipitate is in the form of stable open helices, and enantiomerically pure preparations of the new molecule contain significant numbers of helices possessing the unexpected sense of handedness.

I. Introduction

Dimyristoylphosphatidylcholine (DMPC) and dipalmitoylphosphatidylcholine (DPPC) analogues in which diacetylene groups have been inserted midway in the long hydrocarbon tails self-assemble to yield tubules—stable, hollow crystalline vesicles with a cylindrical morphology, as first reported by Yager and co-workers[1−4] in 1984. The prototypical tubule-forming molecule, 1,2-bis(10,12-tricosadiynoyl)-*sn*-glycero-3-phosphocholine (hereafter DC(8,9)PC, **1**), forms multilamellar tubules in ethanolic solutions that are typically tens of μm in length and about 0.6 μm in external diameter.

Tubules' potential utility in nanofabrication, purification, medical, and encapsulation applications[5−7] fuels much of the interest in current tubule research. Tubules may be aligned with magnetic or electric fields,[8,9] and their capacity to be metal-plated[10] suggests tubules' potential in microelectronics as well as magnetic template applications. The diacetylene groups within the hydrocarbon tails are easily polymerized and may thereby enhance the mechanical, electrical, and optical properties of tubules. Furthermore, tubules' hollowness suggests medical[11] and industrial encapsulation applications,[5−7] as well as filtration and purification applications.[12]

Realization of the full technological potential of tubules requires the ability to optimize their morphology for a given application. Tubule length is controllable over a range of a few μm to hundreds of μm through solvent composition[13] or through the precise control of the rate at which the L_α-phase spherical vesicles are cooled to form the $L_{\beta'}$-phase cylindrical tubules.[14] However, tubule diameter has proven to be insensitive to regulation through control of solvent composition, lipid concentration, cosurfactants, or kinetics.[15] The regulation of tubule diameter is crucial in determining their suitability for technological applications, e.g., if tubules are to be used as encapsulation agents, the diameter directly affects their "payload" capacity, the diffusion rate of encapsulated material, and the spatial dispersion of tubules in aerosols.[11] It has become apparent that any significant modifications of tubule diameters will require new tubule-forming molecules.

The tubule monomer prototype, DC(8,9)PC, is composed of three structural units: (1) a pair of long hydrocarbon tails, each containing an apparently "enabling" diacetylene group in its midsection; (2) a chiral glycerol-derived backbone; and (3) a polar phosphatidylcholine headgroup. Structural modifications thus far have focused on the first and third units. Modifications of the headgroup have involved substitution of the choline portion of DC(8,9)PC by other polar groups.[16,17] For the most part, these substitutions resulted in analogues which either failed to form tubules or which formed tubules closely resembling those formed from DC(8,9)PC. The one exception to this generalization came from the work of Markowitz and co-

(1) Schoen, P. E.; Yager, P.; Priest, R. G. *NATO ASI Ser., Ser. E* **1985**, *102(Polydiacetylenes)*, 223−32.
(2) Yager, P.; Schoen, P. E.; Davies, C.; Price, R.; Singh, A. *Biophys. J.* **1985**, *48*, 899−906.
(3) Schoen, P. E.; Yager, P. *J. Polym. Sci., Polym. Phys. Ed.* **1985**, *23*, 2203−16.
(4) Yager, P.; Schoen, P. E. *Mol. Cryst. Liq. Cryst.* **1984**, *106*, 371−81.
(5) Schnur, J. M. *Science* **1993**, *262*, 1669−76.
(6) Archibald, D. D.; Mann, S. *Chem. Phys. Lipids* **1994**, *69*, 51−64.
(7) Baum, R. *Chem. Eng. News* **1993**, *August 9*, 19−20.
(8) Rosenblatt, C.; Yager, P.; Schoen, P. E. *Biophys. J.* **1987**, *52*, 295−301.
(9) Li, Z.; Rosenblatt, C.; Yager, P.; Schoen, P. E. *Biophys. J.* **1988**, *54*, 289−94.
(10) Schnur, J. M.; Schoen, P. E.; Yager, P.; Calvert, J. M.; Georger, J. H.; Price, R. *Metal-clad lipid microstructures*; U.S. Patent Office, 7 pp, US 4911981 A 900327 US 87-63029 870616, U.S. Navy; 1990.
(11) Johnson, D. L.; Polikandritou-Lambros, M.; Martonen, T. B. *Drug Delivery* **1996**, *3*, 9−15.
(12) Schnur, J. M.; Price, R.; Rudolph, A. S. *J. Controlled Release* **1994**, *28*, 3−13.
(13) Ratna, B. R.; Baral-Tosh, S.; Kahn, B.; Schnur, J. M.; Rudolph, A. S. *Chem. Phys. Lipids* **1992**, *63*, 47−53.
(14) Thomas, B. N.; Safinya, C. R.; Plano, R. J.; Clark, N. A. *Science* **1995**, *267*, 1635−8.
(15) Singh, A.; Chow, G.-M.; Chang, E. L.; Markowitz, M. A. *CHEMTECH* **1995**, *25*, 38−43.
(16) Singh, A.; Marchywka, S. *Polym. Mater. Sci. Eng.* **1989**, 675−8.
(17) Rhodes, D. G.; Frankel, D. A.; Kuo, T.; O'Brien, D. F. *Langmuir* **1994**, *10*, 267−75.

10.1021/ja973933c CCC: $15.00
Published on Web 11/11/1998

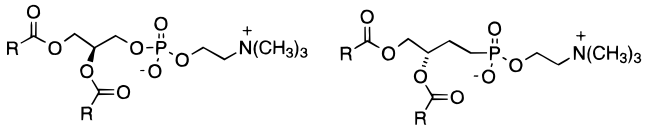

1 **2**

Figure 1. (Left) DC(8,9)PC. (Right) Compound **2**, the phosphonate analogue of DC(8,9)PC.

workers[18] in which choline was replaced by short-chain glycols $HO(CH_2)_nOH$ ($n = 2-4$). Tubule formation in the presence of $CuCl_2$ under rigidly defined conditions of pH and ionic strength led to a bimodal population of tubules having 0.1 and 0.9 μm external diameters, with the former predominating. Slight variations in tubule formation conditions again led to dramatic decreases in tubule yields or formation of tubule of morphologies very close to those formed from DC(8,9)PC.

Changes to the tail section of the parent structure have mostly centered on repositioning the diyne moieties along the tails' lengths,[19,20] but have also included removal of the ester carbonyls (to give ether derivatives)[21,22] as well as addition of polymerizable groups at the tips of the hydrocarbon chains. The results of these structural variations are similar to those found with modifications to the headgroup. While in many cases the modifications seem to have been so subtle as to be unnoticeable (i.e., tubules of virtually identical morphologies to DC(8,9)PC are produced), in other cases the modifications have proven to be sufficiently extreme that tubule formation does not occur; a middle ground of tubule formation with significantly altered morphologies is curiously lacking.

To our knowledge, no modifications of the glycerol backbone of the tubule monomer have been examined. The lack of interest in this portion of the monomer is somewhat surprising given the clear influence which it has on tubule morphology; DC(8,9)PC monomers having an (*R*)-configuration at the middle carbon of the glycerol backbone form tubules having a right-handed sense of winding, while those derived from monomers having an (*S*)-configuration are left-handed.[23]

We report the effects of modifying the glycerol backbone of the DC(8,9)PC monomer through replacement of the oxygen linkage to the phosphate group with a methylene group ($-CH_2-$) to give the phosphonate **2** which, due to the addition of a carbon atom to the three-carbon glycerol backbone, we refer to as the "C4-phosphonate". In light of the strong correspondence between equilibrium tubule handedness and molecular chirality, it seemed reasonable to speculate that the small changes in bond lengths and bond angles associated with this replacement might be sufficiently subtle to allow tubule formation to occur but large enough to produce a noticeable change in morphology, much in the way the action of a lever is "magnified" when working over a long moment arm. Our hopes in this regard were fueled by a number of reports in which similar ($-CH_2-$) for O replacements have been made in phosphorylated natural products, to give phosphonate analogues which serve as inhibitors for enzymes that utilize the natural product as their substrate.[24,25] The success of these analogues in being bound by enzymes which typically exhibit exquisite substrate specificity argues for the close structural similarity of the phosphonate to the phosphate group.

Our synthetic approach to **2** relied on methodology developed by Martin and co-workers for the preparation of phosphonate analogues of phosphatidylcholines.[26] Thus, the acetonide **3** was hydrolyzed to the diol **4**, which was then coupled with 10,12-tricosadiynoic acid to give the ester **5**. Cleavage of the ethyl esters of the phosphonate with bromotrimethylsilane and coupling of the resultant crude phosphonic acid with choline chloride afforded the target **2**.

II. Experimental Section

Synthesis. General Procedures. Methylene chloride and pyridine were distilled and dried from CaH_2 and solid KOH. (*S*)-1,2,4-Butanetriol (99% enantiomeric excess), bromotrimethylsilane, 4-(dimethylamino)pyridine, and choline chloride were purchased from Aldrich. 10,12-Tricosadiynoic acid was purchased from Lancaster. All of these materials were used without any further purification. Silica gel 60 (230−400 mesh) was used for column chromatography. High-resolution mass spectroscopy was carried out by the Washington University Resource for Biomedical and Bio-organic Mass Spectrometry at Washington University, St. Louis, MO.

Diethyl [*O*-3,4-isopropylidene-(*S*)-3,4-dihydroxybutyl]phosphonate (3): prepared by a literature method[27] in 47.2% yield from (*S*)-1,2,4-butanetriol (99% enantiomeric excess).

Diethyl [(*S*)-3,4-dihydroxybutyl]phosphonate (4): prepared by a literature method in 96% yield from the isopropylidene precursor.[26] In our hands, the hydrolysis of the acetonide **3** (using the conditions outlined by Martin) gave diethyl [(*S*)-3,4-dihydroxybutyl]phosphonate **4** that was consistently contaminated with varying amounts of the diastereomeric ethyl methyl [(*S*)-3,4-dihydroxybutyl]phosphonates (hydrolysis and exchange in phosphate and phosphonate esters is greatly facilitated by the presence of a γ-hydroxy group[28]). This was evidenced by the presence of two sets of methyl doublets (for the two possible configurations at phosphorus) at δ 3.76 (d, $J = 6.11$ Hz) and 3.73 (d, $J = 6.17$ Hz). While the mixed phosphonate esters could be partially separated by careful chromatography, this was not done for the bulk of the material which was carried on to **5**; the new chiral center at phosphorus which is formed in the ester exchange reaction is lost in the final product (**2**) and is thus of no concern on a stereochemical basis. Furthermore, the reactivity of the methyl esters in subsequent steps should, if anything, be superior to that of the ethyl esters.

Diethyl [(*S*)-3,4-Bis(10,12-tricosadiynoyloxy)butyl]phosphonate (5): Martin's protocol[26] for preparation of structurally similar phosphonate esters was applied without significant change to the preparation of phosphonate **5**. A solution of 1,3-dicyclohexylcarbodiimide (6.64 g, 32.2 mmol) in dry CH_2Cl_2 (25 mL) was added to a stirred solution of diethyl [(*S*)-3,4-dihydroxybutyl]phosphonate **4** (3.3 g, 14.6 mmol), 10,12-tricosadiynoic acid (10.64 g, 30.7 mmol), (dimethylamino)-pyridine (374.5 mg, 3.07 mmol) and dry CH_2Cl_2 (35 mL), and the solution was stirred under a N_2 atmosphere. After stirring for 14 h at room temperature, the reaction mixture was filtered through Celite, and the filtrate was evaporated to furnish a waxy white solid. The solid was purified by flash chromatography on silica gel using hexane/ethyl acetate (2:1) to give [(*S*)-3,4-bis(10,12-tricosadiynoyloxy)butyl]phosphonate **5** (5.95 g, 46.1%) as a mixture of diethyl and diastereomeric methyl ethyl esters. Common ^{1}H NMR (400 MHz) spectral features of these compounds include δ 5.09 (m, 1H), 4.23 (dd, 1H, $J = 11.9$, 3.7), 4.01 (dd, 1H, $J = 11.9$, 6.06), 2.29 (t, 2H, $J = 7.5$ Hz), 2.28 (t,

(18) Markowitz, M. A.; Schnur, J. M.; Singh, A. *Chem. Phys. Lipids* **1992**, *62*, 193−204.
(19) Singh, A.; Gaber, B. P. *Polym. Sci. Technol. (Plenum)* **1988**, *38*, 239−49.
(20) Ruerup, J.; Mannova, M.; Brezesinski, G.; Schmid, R. D. *Chem. Phys. Lipids* **1994**, *70*, 187−98.
(21) Lee, Y. S.; O'Brien, D. F. *Chem. Phys. Lipids* **1992**, *61*, 209−18.
(22) Rhodes, D. G.; Xu, Z.; Bittman, R. *Biochim. Biophys. Acta* **1992**, *1128*, 93−104.
(23) Singh, A.; Burke, T. G.; Calvert, J. M.; Georger, J. H.; Herendeen, B.; Price, R. R.; Schoen, P. E.; Yager, P. *Chem. Phys. Lipids* **1988**, *47*, 135−48.
(24) Yount, R. G. *Adv. Enzymol.* **1975**, *43*, 1−56.
(25) McClard, R. w. *Tetrahedron Lett.* **1983**, *24*, 2631−34.
(26) Martin, S. F.; Yue-Ling, W.; Wagman, A. S. *J. Org. Chem.* **1994**, *59*, 4821.
(27) Hayashi, H.; Nakanishi, K.; Brandon, C.; Marmur, J. *J. Am. Chem. Soc.* **1973**, *95*, 8749.
(28) Westheimer, F. H. *Acc. Chem. Res.* **1968**, *1*, 70.

2H, $J = 7.5$ Hz), 2.22 (t, 8H, $J = 6.9$ Hz), 1.88 (m, 2H), 1.59−1.24 (m, 62H), 0.87 (t, 6H, $J = 6.9$ Hz). In addition, a complex multiplet due to the CH_2 of P(O)(OR)OCH_2CH_3 (R = Me, Et) at δ 4.12, along with OMe resonances at δ 3.76 (d, $J = 6.11$ Hz) and 3.73 (d, $J = 6.17$ Hz). ^{31}P NMR (195 MHz): 34.39, 33.09, 31.78.

1-[(*S*)-3,4-Bis(10,12-tricosadiynoyloxy)butyl]phosphonic Acid, 2-(*N*,*N*,*N*-Trimethylammonium)ethyl Ester (2). Conversion of diethyl phosphonate **5** to the target phosphatidylcholine analogue **2** followed Martin's protocol for similar transformations without significant changes. Bromotrimethylsilane (0.585 mL, 4.43 mmol) was added over a period of 1 h to a stirred solution of dialkyl [(*S*)-3,4-bis(10,12-tricosadiynoyloxy)butyl]phosphonate (1.5 g, 1.69 mmol) **5** in dry CH_2Cl_2 (3 mL), under a N_2 atmosphere. Six hours after completion of the addition, the reaction mixture was concentrated in vacuo, the residue was brought up in aqueous THF (10%, 6 mL), and the solution was heated at reflux for 1 h. The solvent was removed under reduced pressure, and the residue was dissolved in $CHCl_3$ (15 mL). The $CHCl_3$ solution was dried (Na_2SO_4), filtered, and concentrated under reduced pressure to give 1.39 g of crude phosphonic acid that was utilized without any further purification.

A suspension of the phosphonic acid (1.39 g, 1.67 mmol), choline chloride (1.08 g, 7.71 mmol), and dry pyridine (78 mL) was heated to 60 °C under a N_2 atmosphere. Trichloroacetonitrile (7.2 mL) was added to the 60 °C solution, and the reaction was stirred at that temperature for 20 h. The solvent was removed under reduced pressure, and the residue was dissolved in CH_2Cl_2. Activated carbon was added to the solution, and the mixture was filtered through Celite. The filtrate was concentrated under reduced pressure, and the crude product was purified by flash chromatography on silica gel using $CHCl_3/CH_3OH/H_2O$ (2:0.8:0.15) to give a slightly impure product (270 mg). This material was further purified by acetone precipitation (from chloroform), followed by trituration with acetone to afford 1-[(*S*)-3,4-bis(10,12-tricosadiynoyloxy)butyl]phosphonic acid, 2-(*N*,*N*,*N*-trimethylammonium)ethyl ester **2** (230.5 mg, 14.9%). ^{1}H NMR ($CDCl_3$, 400 MHz): δ 5.14 (m, 1H), 4.36 (m, 2H), 4.27 (dd, 1H, $J = 11.9$, 2.8 Hz), 3.98 (dd, 1H, $J = 12.1$, 7.1 Hz), 3.79 (m, 2H), 3.43 (bs, 9H), 2.24 (m, 12H), 1.88 (m, 2H), 1.26−1.57 (m, 58H), 0.88 (t, 6H, $J = 6.8$). ^{13}C NMR (100 MHz): δ 173.51, 173.41, 77.60, 77.58, 77.39, 76.93, 71.80 (d, $J_{CP} = 15.3$ Hz), 66.86, 65.28, 65.19, 64.85, 57.66, 54.54, 34.43 (d, $J_{CP} = 31.4$ Hz), 31.86, 30.89, 29.61, 29.59, 29.57, 29.54, 29.51, 29.48, 29.45, 29.43, 29.41, 29.39, 29.28, 29.12, 29.07, 28.93, 28.84, 28.80, 28.33, 25.60, 24.87 (d, $J_{CP} = 17.3$ Hz), 22.65, 19.17, 14.10. ^{31}P NMR (195 MHz): δ 24.64. HRMS: calcd for $C_{55}H_{95}NO_7P$ 912.6846, found 912.6828.

III. Physical Characterization

III.a. Methodology. DC(8,9)PC and phosphonate tubules were prepared by adding 1 mg of the lipid to 1 mL of solvent, heating to 50 °C with vigorous stirring, and slowly cooling the clear solutions to room temperature to obtain flocculent off-white precipitates of tubules. The solvent EtOH:H_2O ratio that maximized tubule yields for DC(8,9)PC and the phosphonate **2** were 0.7:0.3 and 0.6:0.4 (v:v), respectively, as determined by centrifuging and desiccating the precipitate to constant mass. The tubule yield was 90.0% for both preparations, and the tubules described throughout this paper were each prepared from their optimal solvent mixture.

Differential interference contrast microscopy (DIC) was conducted with a Nikon Diaphot 300 inverted microscope equipped with 60× and 100× Nomarski objectives, and images were photographed with a Nikon N6006 35 mm camera or digitized with a Dage VE1000 CCD video camera coupled to a high-resolution video capture board. Tubule lengths were tabulated on a Macintosh computer using the public domain NIH Image program, developed at the U.S. National Institutes of Health and available on the Internet at http://rsb.info.nih.gov/nih-image/. Great care was taken to ensure that these length determinations are indeed representative of the tubule formation process and not experimentally induced artifacts. Two factors in particular may lead to distortions of the measured length distribution: (1) mechanically induced fracture of long tubules, creating at least two shorter tubules at the expense of a single long one and (2) the greater likelihood of long tubules to extend beyond the microscope's field-of-view and thus be excluded from counting. To address the first source of potential error, specimens were handled as gently as possible to minimize tubule breakage, which, as we shall elaborate upon presently, is an important consideration with these phosphonate tubules. With respect to the latter source of error, we note that very few tubules exceeded the microscope's 100 μm × 160 μm field-of-view.

Contact- and tapping-mode atomic-force microscopy probes were conducted on a vibrationally and thermally isolated Digital Instruments BioScope, equipped with silicon nitride NanoProbe SPM tips. Local membrane elasticity probes were conducted on this instrument using oxide-sharpened silicon nitride tips.

High-resolution, small-angle X-ray scattering was conducted at beamline X20A of the National Synchrotron Light Source at Brookhaven National Laboratory; 1.6122 Å X-rays were used with an in-plane resolution of 0.0007 Å^{-1}, commensurate with the Ge[1,1,1] analyzer crystal, while out-of-plane resolution was relaxed to 0.008 Å^{-1} to increase signal intensity. Tubule samples of $c \approx 100$ mg lipid/mL were prepared by centrifuging the $c \approx 1$ mg lipid/mL preparation at 10000*g* at 20 °C for 30 min; optical microscopy of the resuspended pellets revealed no discernible change in tubule morphology induced by centrifugation. This concentrated paste was placed in standard 1.5 mm diameter quartz diffraction capillaries, yielding unoriented powder samples.

Tubules polymerize upon exposure to ionizing radiation[29] and acquire a deep purple color in time intervals well below those required for X-ray data acquisition. Radiation damage was minimized by translating 50 mm of the 80 mm capillary continuously through the ≈ 0.5 mm tall collimated X-ray beam during data acquisition, which had the effect of distributing radiation damage throughout an approximately 100-fold larger sample than a stationary sample would present. Accordingly, one should expect a diminution of radiation damage as great as 2 orders of magnitude. Complete data sets were acquired with markedly less sample discoloration and presumably less radiation-induced damage. Each point in reciprocal space was acquired with an integral number of sample translations to ensure that any chance sample inhomogeneities and domain alignments were distributed evenly throughout the reciprocal space scan.

The instrument resolution was deconvolved from the tubule interlamellar (00*l*) peak and fit to the powder average of the scattering from infinite length multilayer tubule structures having outer diameter *D*, wall thickness *T*, and layer spacing *d*. DC(8,9)PC tubules formed in ethanol/water solvent systems are known to be composed of coaxially nested hollow cylindrical lamellae, and we will presently show that this is the case with tubules formed from the phosphonate **2**. These nested layers were assumed to be perfect cylinders, corresponding to membranes with no bending fluctuations, that is, rigid membranes.[30,31] From this model and the measured half-width at half-maximum, we obtained a correlation length ξ which we take to be the mean tubule wall thickness. Because the phosphonate **2** and DC(8,9)PC tubule outer diameters *D* are rather narrowly distributed, determination of the correlation length ξ and the

(29) Thomas, B.; Safinya, C. R.; Plano, R. J.; Clark, N. A.; Ratna, B. R.; Shashidar, R. *Mater. Res. Soc. Symp. Proc.* **1992**, *248*, 83−8.

(30) Safinya, C. R.; Roux, D.; Smith, G. S.; Sinha, S. K.; Dimon, P.; Clark, N. A.; Bellocq, A. M. *Phys. Rev. Lett.* **1986**, *57*, 2718−21.

(31) Roux, D.; Safinya, C. R. *J. Phys. France* **1988**, *49*, 307−0318.

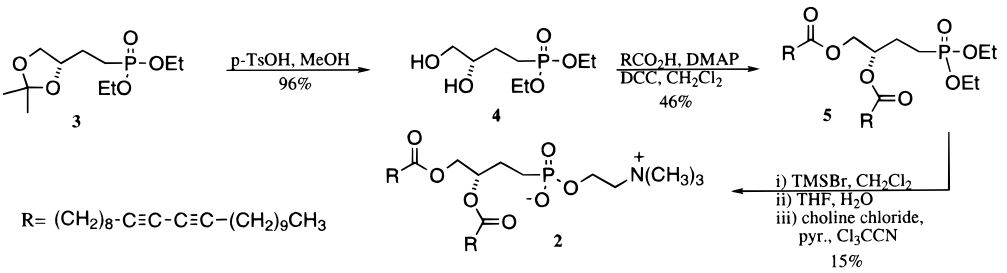

Figure 2. Synthesis of phosphonate **2**.

lamellar spacing *d* permits the determination of the number of lamellae comprising the tubule wall.

III.b. Results. Foremost among our results is that the analogue **2** forms tubules as readily as the prototype, DC(8,9)-PC, thereby proving the hypothesis that DC(8,9)PC's capacity to form tubules will survive the substitution of a ($-CH_2-$) group for the phosphoryl oxygen linking its glycerol backbone to its choline headgroup. The functional similarities of the new molecule to DC(8,9)PC are further borne out by the observations that (1) the ethanol-to-water solvent mixtures that produce optimal tubule yields are similar (0.7:0.3 and 0.6:0.4 (v:v)) for DC(8,9)PC and the phosphonate, respectively; (2) tubule yields are 90% for both molecules in their optimal solvents; and (3) the temperature at which tubules precipitate for both compounds in these solvent mixtures lie within 1 °C of each other. These temperatures vary slightly with different solvent systems but lie between 35 and 39 °C over the manifold of solvent mixtures we investigated.

Comparisons of DC(8,9)PC and phosphonate **2** tubule lengths must take into account the previously mentioned dependencies of tubule length upon solvent composition and cooling rate through the L_α-to-$L_{\beta'}$ phase transition temperature $T_{\alpha\leftrightarrow\beta'}$. We chose the maximum-yield solvent mixture for each molecule and cooled through $T_{\alpha\leftrightarrow\beta'}$ (38 and 37 °C for DC(8,9)PC and the phosphonate **2**, respectively) at the same rate (12.8 °C/h) for both molecules. We found the DC(8,9)PC length to be 25.80 $\pm$ 12.73 μm, whereas tubules made from **2** were 23.48 $\pm$ 11.14 μm. Histograms of DC(8,9)PC and phosphonate tubule lengths are presented in Figure 3.

Despite similarities in tubule length, solubility, phase transition, and yield characteristics, there are several striking differences between phosphonate **2** and DC(8,9)PC tubules. Foremost among these differences are dramatic increases in tubule external diameters and deformabilities: phosphonate tubules have a much greater tendency to flatten when deposited upon a substrate. Flattening-induced distortion requires particular caution when determining tubule diameters, for the products of imaging probes, such as electron or optical micrography, are two-dimensional projections of three-dimensional objects. For an uncollapsed tubule, the width of this two-dimensional projection is equal to the tubule diameter, whereas at the limit of complete tubule flattening the two-dimensional projection width must be reduced by $2/\pi$, or 63%, to estimate the unflattened tubule diameter.

For the reasons just stated, tubule exterior diameters were measured by calculating the perimeter of trapezoidal cross-sectional AFM traces, such as those shown in Figure 4, and dividing by π. We assume the edges of the flattened tubule are actually semicircular and that the trapezoidal cross-section we obtain is a consequence of the AFM tip being unable to probe under the curved edge. That is to say, the trapezoidal profile is the convolution of the finite AFM tip and the curved tubule edge. AFM tip convolution was investigated by scanning

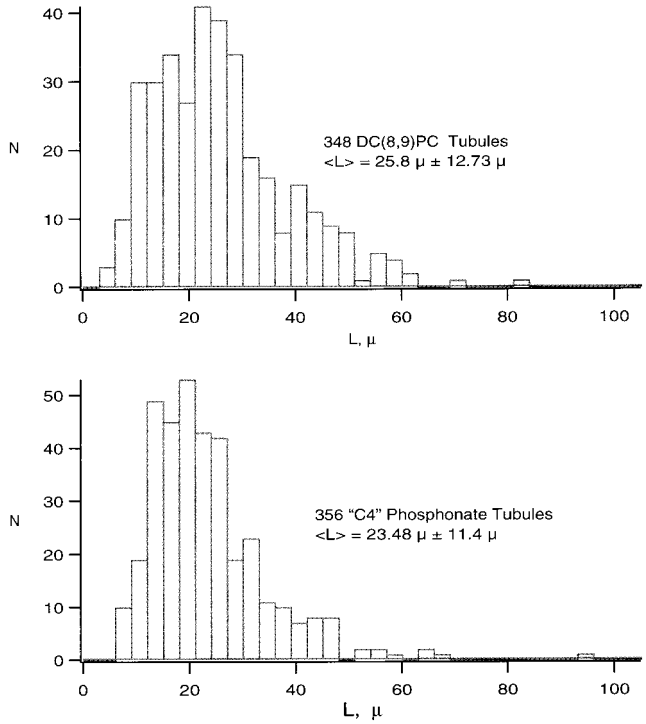

Figure 3. Length histograms for DC(8,9)PC tubules (top) and C4 phosphonate tubules (bottom) cooled at 12.8 °C/h. 348 DC(8,9)PC and 356 phosphonate tubules were measured, yielding mean lengths of 25.80 $\pm$ 12.73 and 23.48 $\pm$ 11.14 μm, respectively.

latex spheres having diameters similar to that of the tubules (0.993 $\pm$ 0.021 μm, Duke Scientific Corporation) and calculating the sphere diameters from the AFM-derived trapezoid perimeters. The diameters so determined from 10 spheres were within 0.8% of the NIST-traceable value. We remark further that for tubules the trapezoid sides represent a small portion of the total perimeter and a very much smaller portion of the total perimeter than is the case with the latex spheres. Worst-case scenarios for measurement error yield values within a few percent of those we report above. Our AFM determination of the mean DC(8,9)PC tubule diameter is 0.554 $\pm$ 0.053 μm, in agreement with other reports in the literature;[4] thus, it seems our protocol provides accurate tubule diameter determinations. This protocol reveals the mean phosphonate tubule external diameter to be 1.182 $\pm$ 0.135 μm, a significant 2.06-fold increase over that of DC(8,9)PC tubules.

As is the case with DC(8,9)PC, phosphonate tubules appear to be composed of helically wound multilayered ribbons having a length:width ratio on the order of 100:1. Helices are chiral, and the *R*-enantiomer of DC(8,9)PC is known to yield tubules whose exterior helical traces are left-handed, while the *R*-enantiomer produces tubules with a right-handed exterior trace. We were quite surprised when optical and atomic-force mi-

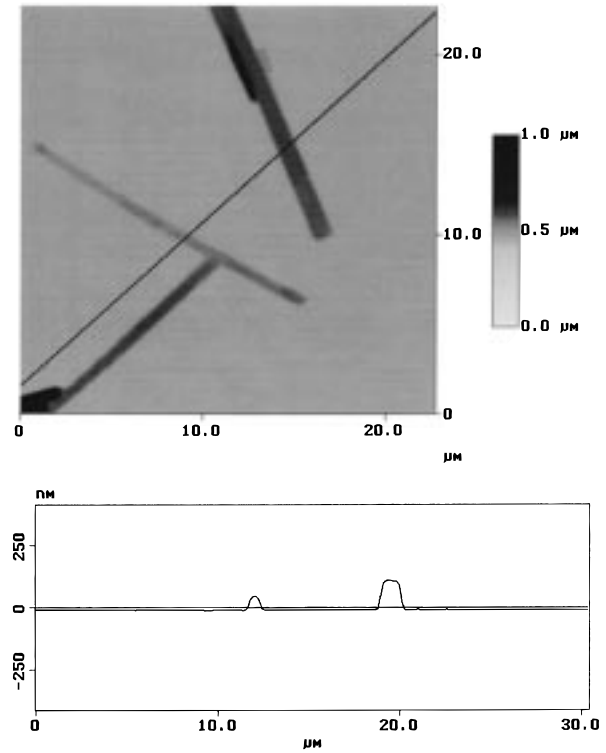

Figure 4. Contact-mode AFM of DC(8,9)PC and C4 phosphonate tubules. The glass substrate was divided into two regions that were masked alternately as suspensions of each tubule were deposited and air-dried. Top: two DC(8,9)PC tubules in the lower-left-hand quadrant of micrograph and a single, larger phosphonate tubule in the upper-right-hand quadrant. Bottom: the height along the trace drawn through the micrograph. Note the different scales for the horizontal and vertical axes.

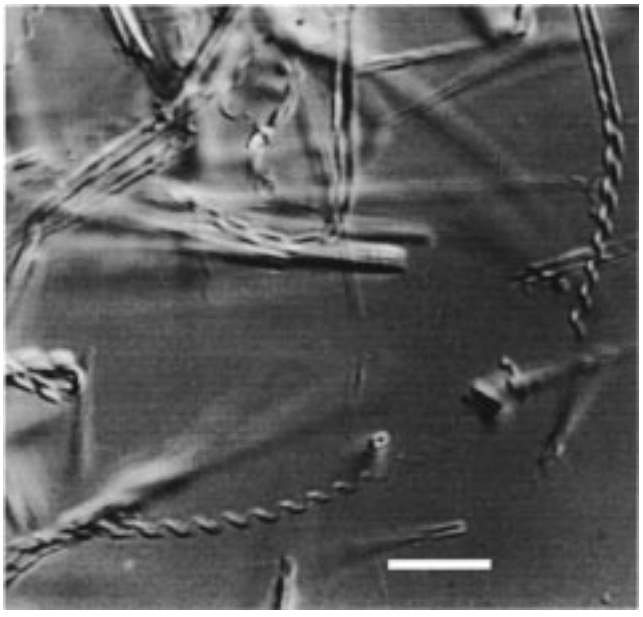

Figure 5. Differential interference contrast microscopy image of coexisting right-and left-handed C4 phosphonate helices, found at the bottom and far right-hand side of the figure, respectively. The microscope focal plane is on the near side of the helices. The scale bar is 5 μm.

croscopy revealed that our enantiomerically pure phosphonate **2** contains right- and left-handed helices, as shown in Figure 5. While stable open DC(8,9)PC helices have been reported in 2-propanolic solvent systems,[32] electron microscopy revealed

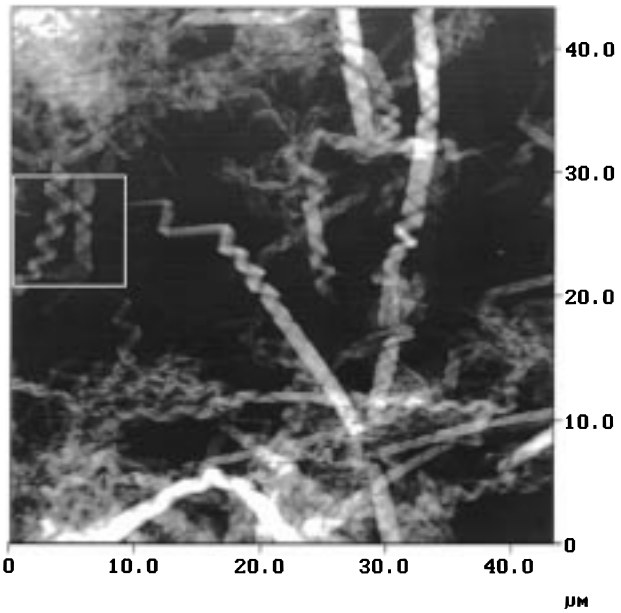

Figure 6. Contact-mode AFM of C4-phosphonate tubules, showing the "near" and "far" side of the ribbon's helical winding, which we interpret as arising from highly deformable phosphonate tubule walls. The region contained in the box is represented in pseudo-three-dimensional perspective in Figure 7.

only the anticipated right-handed helices; with the phosphonate **2** the ratio of left- to right-handed helices, N_L/N_R, appears to be sensitive to the rate of formation, addressed in a forthcoming paper.

The surprising presence of left- and right-handed helices of course demands careful examination of experimental conditions. By virtue of the synthesis, carrying a starting material of 99% enantiomeric excess through a stereochemically unambiguous sequence of reactions, it is highly unlikely the presence of right- and left-handed helices is due to enantiomeric contamination. The tubule formation environment is achiral, so we focus our attention upon the AFM and optical microscopy probes yielding these unexpected results.

One might expect the three-dimensional height maps rendered by AFM to lead quickly to helix handedness determination, but a number of factors conspired to prevent this. First, tubules in suspension are quite mobile and could not be imaged by the scanning tip. AFM probes of phosphonate tubule suspensions deposited onto substrates and air-dried failed to resolve helix handedness due to the extraordinary phosphonate tubule deformability: unlike DC(8,9)PC tubules, air-dried phosphonate helices are so flattened that the "near" and "far" sides of the exterior helical traces are observed, yielding the achiral "zigzag" patterns found in Figure 6. These achiral zigzag patterns are, in fact, quite similar to the two-dimensional images produced by transmission electron microscopy (TEM), which are in general uninterpretable with respect to tubule handedness. Height-averaging alternate portions of the zigzag pattern failed to reveal which were closest to the viewer, for the height differences so obtained were of the same magnitude or less than that of the ribbon roughness. For these reasons, even open helices, such as those seen in the left-hand side of the box drawn in Figure 6, were beyond our capacity to resolve. The remarkable extent of phosphonate tubule flattening and ribbon roughness are shown in Figure 7, a pseudo-three-dimensional representation of the boxed area in Figure 6.

(32) Georger, J. H.; Singh, A.; Price, R. R.; Schnur, J. M.; Yager, P.; Schoen, P. E. *J. Am. Chem. Soc.* **1987**, *109*, 6169−75.

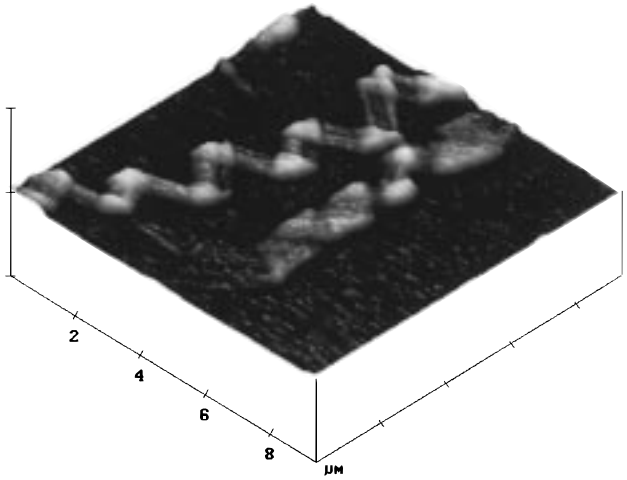

Figure 7. Pseudo-three-dimensional perspective of the boxed area of Figure 6. The highly deformable ribbon lies so flat upon the substrate and is so rough that an unambiguous determination of helix handedness is not possible, even after height-averaging alternating helix segments.

Resolvable AFM height maps were finally obtained, however, from helices that were first deposited and air-dried upon a glass substrate, then immersed in water, and finally imaged in an AFM fluid cell. Rehydrating the phosphonate helices unflattened them, but they adhered to the glass substrate while being probed by the AFM tip. Figure 8 shows left- and right-handed phosphonate helices obtained through fluid-cell AFM scanning.

Somewhat surprisingly, the two-dimensional transmission-mode images yielded by optical microscopy proved to be a sensitive probe of tubule handedness. This is so for two reasons: First, like the fluid-cell AFM probe (and unlike in vacuo TEM), phosphonate helices are examined in solution and, hence, as unflattened helices. Second, the high-magnification optics we utilized have an extremely narrow focal plane, permitting placement of the narrow focal plane unambiguously on the side of the helix lying closest to the viewer, thereby enabling unequivocal assignment of helix handedness.

This technique will fail, of course, if the "near" and "far" sides of the helix are confused by the microscopist. The two-dimensional images rendered by optical microscopy may be thought of as the intersection of the microscope focal plane with the helix, which lies perpendicular to the viewing axis. If the focal plane intersects the helix on the side nearest the viewer, handedness may be assigned through comparison of the ribbon winding pattern with, say, the grooves of a machine screw. If, however, the focal plane is mistakenly placed at the far side of the helix, the intersection will yield a two-dimensional pattern that is the reverse of that obtained at the near side, thereby rendering the incorrect handedness.

At the high numerical apertures employed in our measurements, only the downstream (that is, nearest the objective) side of the helical winding can be imaged reliably, irrespective of through-focus position. Occasionally, phosphonate helices with diameters large enough to permit unambiguous placement of the microscope focal plane on either the near or far side of the helix are found; through-focusing these helices produces the anticipated shift in apparent handedness, as shown in Figure 9 (top). At the other extreme, desiccated phosphonate helices are flat enough that both helix sides are simultaneously in focus, yielding zigzag patterns that, like TEM images, are uninterpretable with respect to handedness assignment (see Figure 9 (bottom)). We emphasize that only the intermediate case, that is, unflattened, hydrated phosphonate tubules of diameter ≈ 1 μm, were used in handedness determination, and that due care was exercised to image only the helix side nearest the objective.

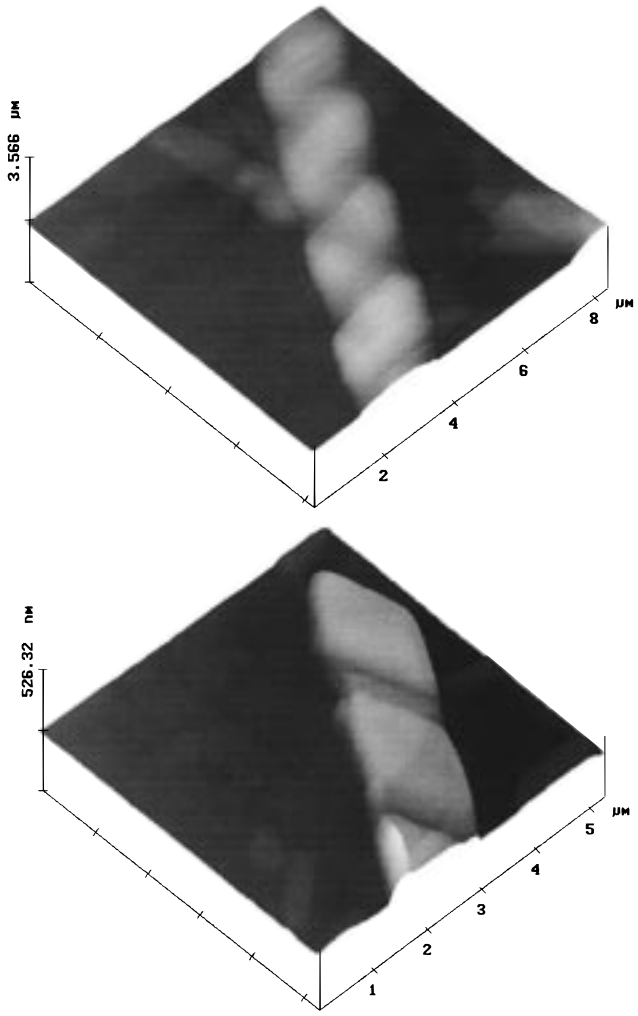

Figure 8. Pseudo-three-dimensional perspective of right-handed (top of figure) and left-handed phosphonate helices (bottom of figure) in the same phosphonate preparation, obtained with underwater contact-mode AFM.

We now consider the possibility that the specialized microscopy technique employed, differential interference contrast (DIC) microscopy, can generate artifacts leading to errors in tubule handedness assignment. DIC utilizes variations in the specimen refractive index by combining two slightly displaced images along the so-called DIC optical translation axis. This displacement brightens regions where the refractive index increases along the DIC optical axis and vice versa. These effects are most pronounced at refractive index discontinuities, such as the object/water interface, particularly if this interface is an edge perpendicular to the DIC axis. The composite image appears to be illuminated obliquely, which can impart a false three-dimensional character to the image.

To test whether the orientational dependencies of DIC image combination and edge enhancement can create misleading artifacts in the helical ribbon pattern, a microscope stage was constructed to rotate the specimen about the viewing axis, that is, through the DIC axis. It was found that the apparent sense of helix handedness does not change with helix orientation in the illumination field; isolated helices rotated 180° with respect to the DIC axis maintain their apparent sense of handedness throughout the rotation. However, as one should expect, the sharpness of the helix features do vary somewhat with sample orientation.

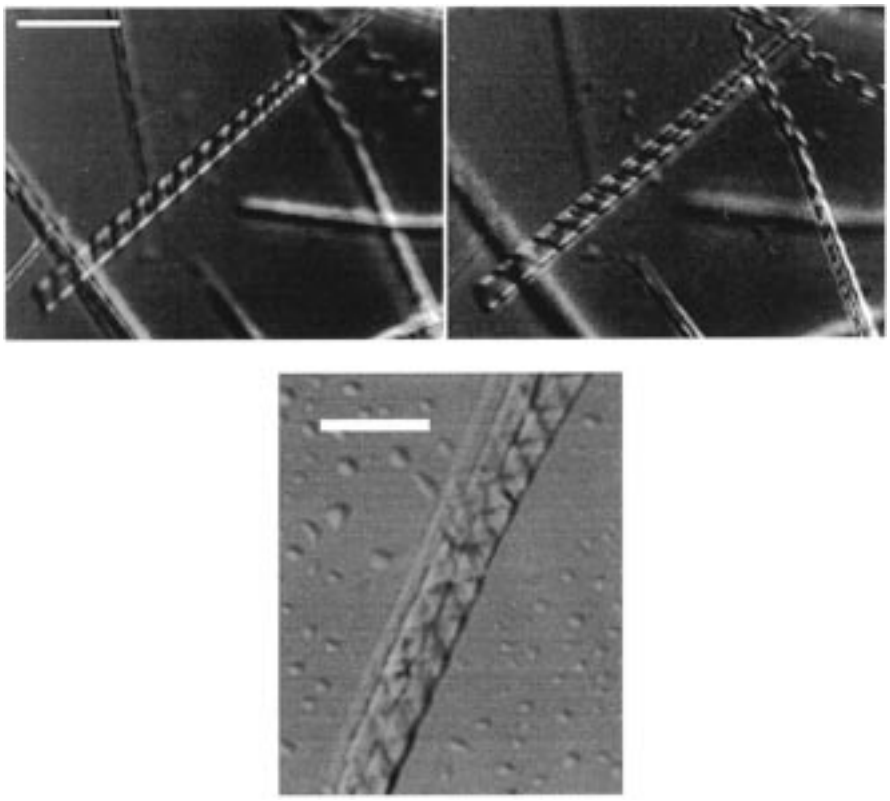

Figure 9. Top: two frames from a DIC optical microscopy through-focus sequence of a large hydrated (unflattened) phosphonate tubule, showing an apparent shift in handedness as the focal plane traverses the tubule axis, as discussed in the text. Bottom: DIC optical micrograph of three parallel, desiccated (flattened) phosphonate helices, in which the near and far sides of the two rightmost helices are simultaneously in focus. The leftmost helix, lying partially under the other two, is not quite in focus. The scale bar is 5 μm in both images.

The extent of phosphonate tubule deformability was investigated through comparative force-modulation AFM measurements of local membrane elasticity. In this technique, the AFM tip is forced down upon the sample and the amplitude of the cantilever tip deflection vs height above the sample is measured. The magnitude of the oscillating cantilever's deflection as it is pushed onto the sample is inversely related to the extent of indentation induced in the sample. As the AFM tip approaches, a "soft" sample will deform with little resistance, causing only a small change in the amplitude of the oscillating cantilever's deflection. Under the ambient conditions in which these studies were conducted, the cantilever tip had to be driven with 1.77× greater amplitude with phosphonate tubules to obtain the same cantilever deflection obtained with DC(8,9)PC tubules, indicating that the phosphonate tubule wall is significantly more elastic. We argue below that the greater deformability observed in phosphonate tubule walls is attributable to the presence of fewer lamellae, although significant contributions to the deformability from possibly different bulk and shear moduli in the phosphonate lamellae cannot be excluded.

DIC microscopy under sample conditions of high-temperature homogeneity and very slow cooling reveals that the dominant DC(8,9)PC tubule assembly mechanism is the rapid growth of helical ribbons from spherical vesicles, which is followed by a much slower ribbon widening that leads to closure of the helices into cylindrical tubules, finally leaving the prominent helical ridge upon the tubule exterior. It is assumed that no subduction of one ribbon edge under the other occurs in this process, that is, that the ribbon width and the helical pitch are matched through the cessation of ribbon widening upon closure. We utilized AFM to investigate the relationship between helical pitch, ribbon widths, and the mechanical resilience of the multilayer ribbons composed of the two molecules.

Helical pitch is expressed in terms of the ribbon width and the angle of the ribbon edge with respect to the cylindrical axis. The C4 phosphonate tubule pitch angle is found to be 58.13° ± 2.84°, commensurate with the widely accepted[4] DC(8,9)PC value of 60°. To maintain cylinder closure, the ribbon width must double as the tubule diameter doubles at a fixed pitch angle. Phosphonate and DC(8,9)PC ribbon widths were determined directly, whenever possible, from intact tubules in which both ribbon edges could be unambiguously detected. This optimal situation is rather rare, for close examination of the tubule's barber-pole winding almost always suggests the possibility of subduction throughout the tubule's length. We opportunistically measured the ribbon widths of isolated ribbon fragments as they were found. These fragments appear to be the result of tubule breakage from handling, as evidenced by their sharp edges and/or ends, and we took care to examine only the apparently undamaged portions of these fragments. The larger phosphonate ribbon width scales well with the 2.06-fold phosphonate tubule diameter increase: while 16 isolated DC(8,9)PC ribbons yielded a mean width of 0.605 ± 0.049 μm, 30 isolated C4 phosphonate ribbons yielded a mean width of 1.176 ± 0.028 μm, a 1.94-fold increase. This result indicates that, as with DC(8,9)PC tubules, no ribbon subduction occurs in phosphonate tubules. The number of specimens reported here (that is, 16 DC(8,9)PC ribbons vs 30 C4 ribbons), however, is somewhat misleading, for a far more exhaustive search was required to find DC(8,9)PC ribbon fragments.

The far greater number of phosphonate tubule fragments found after even moderate sample handling indicates that phosphonate tubules are more fragile than DC(8,9)PC tubules. The zigzag pattern seen on collapsed phosphonate tubules strongly suggested that phosphonate tubules are thinner-walled than those made from DC(8,9)PC (that is, consisting of fewer

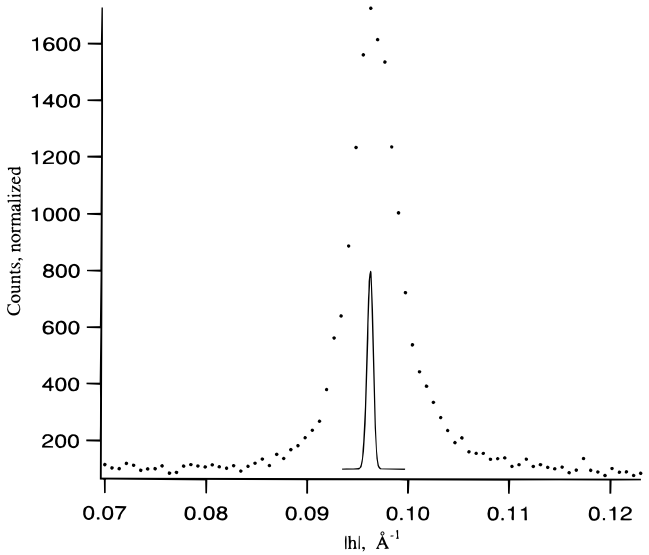

Figure 10. High-resolution small-angle X-ray scattering from a C4 phosphonate tubule preparation. The phosphonate (00l) peak is centered at 0.096 21 Å^{-1}, indicating an interlamellar spacing of 65.31 Å. Analysis of the peak width reveals a correlation length $\xi = 198.2$ Å. The narrow solid curve beneath the peak is the 0.0007 Å^{-1} fwhm instrument resolution, drawn to a different scale.

lamellae) and this speculation is supported by the AFM determination of greater local deformability normal to the phosphonate tubule axis.

Precise characterization of C4 phosphonate and DC(8,9)PC tubule wall thickness (as well as interlamellar spacing) is provided by small-angle X-ray scattering (SAXS). The C4 phosphonate tubule (00*l*) peak of Figure 10 is centered at $|l_0| = 4\pi \sin(2\theta/2)/\lambda = 0.09624$ Å^{-1}, implying an interlamellar spacing $d = 65.29$ Å. Despite a doubling of tubule diameter, phosphonate interlamellar spacing is only slightly larger than the 62.97 Å spacing found in DC(8,9)PC tubules.[14] In light of this similarity to DC(8,9)PC, it is reasonable to assume the phosphonate intralamellar structure is fundamentally that found previously for DC(8,9)PC;[33] the remarkably small change in interlamellar spacing suggests strongly that the interlamellar forces which determine the spacing *d* are unchanged in the new tubule structure.

Peak shape analyses yield correlation lengths $\xi = 431.08$ Å and $\xi = 207.0$ Å for the DC(8,9)PC and the C4 phosphonate tubules, respectively. Due to the narrow dispersion of tubule diameters for tubules made from both molecules, we interpret these values to be equivalent to the tubule wall thickness *T*. The ratio of tubule wall thickness to interlamellar spacing is the number *n* of bilayers composing the tubule; we find *n* to be 6.9 for DC(8,9)PC and 3.2 for the C4 phosphonate. That phosphonate tubules are composed of significantly fewer lamellae than DC(8,9)PC tubules and yet have a greater external diameter can only be attributed to a significantly larger intrinsic cylindrical radius of curvature of the phosphonate lamellae. We emphasize that while our X-ray data permits accurate determinations of interlamellar spacing and the associated correlation length, it lacks the higher-order reflections required to determine the thickness of a *single* lamella.

IV. Conclusion

The tubule-forming capacity of DC(8,9)PC is unhindered by the replacement of a ($-CH_2-$) group for the phosphoryl oxygen linking its glycerol backbone and choline headgroup. This subtle modification, however, has had dramatic effects upon several tubule properties, most notably tubule external diameter, which is 2.06 times greater for the phosphonate. Interestingly, while small-angle X-ray scattering shows virtually no difference in interlamellar spacing, correlation lengths show the phosphonate tubules to be thinner-walled, that is, composed of fewer coaxially nested lamellae. Because the phosphonate tubules are thinner-walled, the observed diameter increase must be due to a significantly larger intrinsic radius of curvature of the phosphonate lamellae over those of DC(8,9)PC.

The lower number of lamellae in phosphonate tubules influence physical properties in the expected ways. First, phosphonate tubules are more fragile, as evidenced by the comparatively large number of tubule fragments observed after moderate sample handling. Second, the thinner-walled phosphonate tubules are more deformable, as seen by the zigzag pattern evident on completely collapsed phosphonate tubules. Finally, AFM measurements show the phosphonate tubules to have a significantly higher local elasticity normal to the tubule surface.

From a practical standpoint, it is worth noting that the decrease in phosphonate tubule wall thickness means that the inner diameters of the C4 phosphonate tubules are, if anything, slightly more than the 2.06-fold increase in external diameter over the DC(8,9)PC tubules. The control of tubule internal and external diameters, particularly without depending upon the presence of heavy metal cations and stringent pH control, is potentially important for technological reasons, in addition to theoretical ones. For example, the mild formation conditions under which DC(8,9)PC and phosphonate tubules form suggest their suitability as pharmaceutical encapsulation agents. Parameters that must be tightly controlled in such applications are (1) the tubule's "payload" capacity, (2) the outward diffusion rate of the encapsulated material, and (3) the ability to situate them in the desired location within the body. The slightly more-than-doubled inner diameter should lead to a quadrupled payload capacity, and the encapsulant diffusion rate should be significantly higher due to the phosphonate tubule's larger hollow core. The ability to place tubules in the body depends, to a large extent, upon the tubule's diameter. For example, the mean deposition distance of aerosolized fibers of length *L* and diameter *D* subjected to shear flow, the conditions of inhalation therapies, has been found to be of the form[34]

$$x \propto D^{5/6} L^{1/6}$$

which is dominated by the diameter.

Finally, the observation of stable right- *and* left-handed helices in our enantiomerically pure phosphonate **2** preparations has profound implications regarding the roles that molecular tilt and chirality play in tubule formation. The experimental results that a comprehensive theory must explain are (1) the generation of helices of only one sense of handedness from enantiomerically pure DC(8,9)PC preparations; (2) helices of both senses of handedness arising from mixed-enantiomer DC(8,9)PC preparations;[35] and the result reported in this manuscript, (3) the generation of helices of both senses of handedness from enantiomerically pure phosphonate preparations.

(33) Caffrey, M.; Hogan, J.; Rudolph, A. S. *Biochemistry* **1991**, *30*, 2134−46.

(34) Störber, W. *Dynamic Shape Factors of Non-Spherical Aerosol Particles*; Störber, W., Ed.; C. C. Thomas: Springfield, IL, 1972; pp 249−289.

(35) Spector, M. S.; Selinger, J. V.; Schnur, J. M. *J. Am. Chem. Soc.* **1997**, *119*, 8533−8539.

Theories advanced by Selinger et al.[36] have been used to explain outcomes (1) and (2) above. In these theories, chiral packing of the molecules composing the bilayer is responsible for imparting a twist to the ribbon, and this twist ultimately leads to helix formation. The magnitude of this twist also determines tubule diameter. As packing efficiency in a pure bilayer decreases with the introduction of the opposite enantiomer, the magnitude of twist is reduced, and tubule diameter is predicted to increase, diverging to infinity at the racemic concentration. However, enantiomer-mixing experiments designed to test this prediction (experiment (2), above) fail to reveal any dependence of tubule diameter upon enantiomeric excess;[35] indeed, tubules of unchanged diameter are produced by racemic DC(8,9)PC mixtures.[23] That left- and right-handed helices are seen in mixed-enantiomer preparations has nevertheless been interpreted as evidence for the chiral-packing model: under these interpretations, the driving force for chiral packing is sufficiently powerful that a spontaneous enantiomeric separation occurs prior to tubule formation, which then proceeds as prescribed by the chiral-packing theory.

Under competing chiral symmetry-breaking theories,[37] the origin of membrane chirality is *not* chiral intermolecular interaction but rather a collective tilt of the molecules with respect to the membrane normal. Within the framework of collective tilt-based theories, chiral membranes may result even from achiral molecules. This is an important point, for chiral-packing theories state that chiral interactions are averaged to zero in racemic mixtures, and yet tubules are seen to form. To provide the chiral interactions required by packing theories, a spontaneous separation of enantiomers must be postulated to precede tubule formation.

Given the stereochemically unambiguous nature of the phosphonate synthesis and the fidelity of optical and AFM microscopy probes in determining helix handedness, the observation of left- and right-handed helices in enantiomerically pure phosphonate **2** must then be taken to support chiral symmetry-breaking models of tubule formation. In one way, tilt-driven chiral symmetry-breaking models fit experimental observation (2), the DC(8,9)PC mixed-enantiomer experiment producing left- and right-handed helices, better than do chiral-packing ones. No dependence of tubule diameter upon enantiomeric excess is predicted, and the tilt mechanism that produces chiral membranes does not depend on composition: tubules may form in racemic mixtures without prior enantiomeric separation. Furthermore, as is the case with the phosphonate **2**, a "mixed"-handedness population is the expected result.

Despite the extreme similarity of DC(8,9)PC and the phosphonate **2**, enantiomerically pure preparations of each present results that can only be accounted for by competing theories. The uniform helix handedness found in enantiomerically pure DC(8,9)PC preparations is traceable to molecular dimensions in chiral-packing theories, whereas the "mixed"-handedness phosphonate results are more consistent with the collective tilt of bilayer ensembles in chiral symmetry-breaking models.

In the purely tilt-based chiral symmetry-breaking models, the membrane constituents are achiral, which is not the case for DC(8,9)PC or the phosphonate **2**. Speculating upon the effects that molecular chirality might exert upon the tilt distributions present in chiral symmetry-breaking models, and thence the ratio of right- to left-handed helices, inevitably leads one to integrate key aspects of chiral-packing theories. For example, the contradictory results with enantiomerically pure DC(8,9)PC and the phosphonate **2** (outcomes (1) and (3) above, uniform and "mixed"-handedness, respectively) may be explained by postulating that a bias, whose origins lie in molecular chirality, influences the tilt direction chosen by the bilayer membrane ensemble. In DC(8,9)PC, this bias dominates, leading to tubules of a single handedness, whereas in the phosphonate **2** the effects of the chiral tilt bias are diminished, permitting the generation of left- and right-handed helices from enantiomerically pure **2**. Any disparity in DC(8,9)PC and phosphonate chiral tilt biases must lie in the differences between the molecules, and as we argued above, the O $\rightarrow$ CH_2 substitution leading to the phosphonate is quite close to the chiral center of the molecules; hence it is reasonable to expect such changes in chiral properties.

The tilt bias we postulate may be related to the packing efficiency found in chiral-packing theories, for we observe that the increase in phosphonate tubule diameter is concurrent with the creation of helices of both senses of handedness. If we interpret the "mixed"-handedness found in phosphonate samples as indicating a diminished prominence of molecular chirality, then the increased tubule diameter somewhat parallels chiral-packing theory predictions about reduced packing efficiency leading to increased tubule diameter. However, this conveniently drawn parallel between the two theories may be misleading, for it does little to explain the DC(8,9)PC enantiomer-mixing experiments (result 2 above), in which chiral interactions must be averaged to zero, and yet no significant change in tubule diameter is found. So, while chiral-packing theories cannot explain the coexistence of left- and right-handed helices found in enantiomerically pure phosphonate preparations, achiral collective-tilt theories fail to explain the uniformly handed helices produced by enantiomerically pure DC(8,9)PC. The surprising chirality/helical handedness obtained with phosphonate **2** and its similarity to DC(8,9)PC present a remarkable opportunity to probe the relationship between chirality and tubule handedness.

Acknowledgment. Portions of this work were executed at beamline X20A of the National Synchrotron Light Source at Brookhaven National Laboratory, administered by the United States Department of Energy. B.N.T., J.E.K, and C.M.L. were supported in part by the Research and Training Program of the Exxon Education Foundation. C.L.C. and C.M.L. were supported by a University of Wyoming Grant-In-Aid. High-resolution mass spectra were obtained by the Washington University Resource for Biomedical and Bio-organic Mass Spectrometry at Washington University, St. Louis, MO.

JA973933C

(36) Selinger, J. V.; MacKintosh, F. C.; Schnur, J. M. *Phys. Rev. E: Stat. Phys., Plasmas, Fluids, Relat. Interdiscip. Top.* **1996**, *53*, 3804−18.

(37) Seifert, U.; Shillcock, J.; Nelson, P. *Phys. Rev. Lett.* **1996**, *77*, 5237−5240.